The Journal of the Oceanological Society of Korea
Vol. 25, No. 4, pp. 161-181, December 1990

Numerical Simulations of the Storm Surges in the Seas Around Korea

IM SANG OH AND SEONG IL KIM
Department of Oceanography, Seoul National University, Seoul 151-742, Korea

韓國 近海의 暴風 海溢 數値 시뮬레이션

吳林象 · 金成一
서울大學校 海洋學科

A numerical model is established in order to simulate the storm surges which were observed in the seas around Korea during typhoon and winter storm periods. The typhoons are Brenda (1985), Vera (1986) and Thelma (1987). The winter storm period is January 1-6, 1986. The simulated surges for the typhoon periods show good agreements with the recorded ones for the periods at the Korean coasts, but those for the winter strom show fair agreements in general tendencies, not in details.

The model simulation in open sea shows a positive sea level near the typhoon center and a negative sea level behind the typhoon. The positive surge seems to be due to the low pressure near a typhoon center and the negative one due to the wind stresses of the typhoon. The negative sea level is usually in the form of an elongated gyre. In the gyre, there is a cyclonic circulation of sea water, in which the pressure gradient force induced by the circular depression of the sea surface is balanced by the Coriolis force in readjusting stage.

颱風 및 溫帶性 低氣壓 통과시 韓國 沿岸에서 觀測된 海溢을 시뮬레이션 하기 위하여 數値모델을 開發하였다. 사용된 颱風은 브렌다(Brenda, 1985), 베라(Vera, 1986), 셀마(Thelma, 1987)이고, 低氣壓은 1986년 1월 1-6일 사이에 발달한 것이다. 颱風 통과시 시뮬레이션의 結果는 觀測値와 잘 일치하나 溫帶性 低氣壓시는 상당한 差異를 보였다.

시뮬레이션에서 颱風 中心 부근에서는 低氣壓 效果에 의해 陽의 海面이, 그리고 颱風 後側에는 바람 응력에 의해 陰의 海面이 나타났다. 陰의 海面 領域은 길게 늘어진 gyre 모양을 하며 여기에는 反時計 방향의 海水 循環운동이 존재한다. 이 운동은 颱風이 지나간 후 海面이 再整理되는 단계에서 海面 傾斜로 인한 壓力 傾度力과 코리오리의 힘이 均衡을 이루고 있다.

I. INTRODUCTION

Rapid variations of air pressure with strong winds occur during typhoon or extratropical cyclone passages in the seas around Korea. The typhoons affecting the Korean Peninsula originate in the North Pacific (5-20°N., 125-155°E). The number of these tropical cyclones is about 25 a year, among these 2 or 3 pass the adjacent seas to Korea in summer (Korean Central Meteorological service, 1984). In winter many of the extratropical cyclones developed in China cross the Yellow Sea and affect the Korean Peninsula. Northwesterly and northerly winds are dominant during the winter monsoon in this area. These meteorological events induce rapid disturbances of sea surface in a short time i.e., storm surges.

The storm surges of Korea have been studied by data analysis (Hwang, 1971; Chu, 1987; Oh, et al., 1988) and by numerical medelling (Korea Ocean Research and Development Institute,

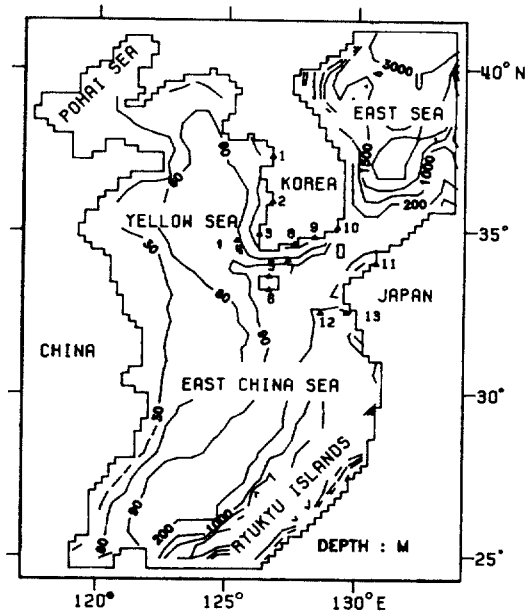

Fig. 1. Model area covering the Yellow, East China and part of the East Seas. Small triangles indicate the position of the sea level stations; 1 (Inchon), 2 (Kunsan), 3 (Mokpo), 4 (Daeheugsan), 5 (Cheju), 6 (Seogwipo), 7 (Keomundo), 8 (Yeosu), 9 (Chungmu), 10 (Pusan), 11 (Simonoseki), 12 (Fukue) and 13 (Nagasaki).

1985, 1986; Choi, 1986). Through these data analysis, following surge characteristics were found: maximum storm surges on the southern coast of Korea were caused by typhoons in summer, while on the western coast they were caused by northwesterly monsoon wind in spring and winter (Hwang, 1971). The ranges of the maxima of the significant surges were 83-109 cm in the western coast and gradually decreased 43-90 cm for the southern coast and 30-68 cm for the eastern coast of Korea (Chu, 1987). The conspicuous figure of typhoon surge on the southern coast of Korea is that a positive surge is followed by a downward bend (or a negative surge in some place) after typhoon passage. This phenomenon is more clear in the western station, such as Cheju, Seogwipo and Keomundo (see Fig. 1 for these locations) than in the eastern stations, Pusan and Ulsan (Oh, *et al.*, 1988).

The numerical model studies above have been focused on surge hindcast. Choi (1986) established a numerical model which was applied to the typhoons Carmen and Wendy of 1978. He compared the calculated results with the sea level data from several tidal stations.

In the present study, a numerical model which can be used for computing surges due to summer typhoons and extratropical winter storms is developed. We applied the model to the storm surges which are induced by the typhoons, Brenda (1985), Vera (1986) and Thelma (1987), and to the extratropical winter cyclone of January 1-6, 1986.

We also investigate the surge characteristics and dynamic responses of currents to the meteorological forcings in the shallow and coastal areas which are believed to be accociated with sea level variations in open sea.

II. THE MODEL

A. The Governing Equations

The vertically-integrated equations of motion and that of continuity are used. Equations are basically nonlinear in advection and quadratic bottom friction terms.

The equation of continuity in spherical coordinates (θ in east-west direction, and ϕ in north-south direction) is

$$\frac{\partial \eta}{\partial t}+\frac{1}{R\cos\phi}\left\{\frac{\partial}{\partial \theta}(UH)+\frac{\partial}{\partial \phi}(VH\cos\phi)\right\}=0. \tag{1}$$

The equations of motion are as follows,

$$\frac{\partial U}{\partial t}+\frac{U}{R\cos\phi}\frac{\partial U}{\partial \theta}+\frac{V}{R\cos\phi}\frac{\partial (U\cos\phi)}{\partial \phi}$$

$$-2\omega\sin\phi V=\frac{-g}{R\cos\phi}\frac{\partial \eta}{\partial \theta}-\frac{1}{\rho R\cos\phi}\frac{\partial P_a}{\partial \theta}$$

$$+\frac{1}{\rho H}(\tau\theta_s-\tau\theta_B)+A\nabla^2 U, \tag{2}$$

$$\frac{\partial V}{\partial t}+\frac{U}{R\cos\phi}\frac{\partial V}{\partial \theta}+\frac{V}{R}\frac{\partial V}{\partial \phi}+\frac{U^2\tan\phi}{R}$$

$$+2\omega\sin\phi\, U = -\frac{g}{R}\frac{\partial\eta}{\partial\phi} - \frac{1}{\rho R}\frac{\partial P_a}{\partial\phi}$$

$$+\frac{1}{\rho H}(\tau\phi_s - \tau\phi_B) + A\nabla^2 V, \qquad (3)$$

Here, vertically-averaged velocity components, U and V are defined as follows,

$$U = \frac{1}{H}\int_{-h}^{\eta} u\, dz, \quad V = \frac{1}{H}\int_{-h}^{\eta} v\, dz, \qquad (4)$$

and the simbols have the following meanings,

$$\nabla^2 = \frac{1}{R^2\cos^2\phi}\frac{\partial^2}{\partial\theta^2} + \frac{1}{R^2}\frac{\partial^2}{\partial\phi^2} - \frac{\tan\phi}{R^2}\frac{\partial}{\partial\phi}. \qquad (5)$$

u, v: eastern and northern components of horizontal current, respectively,
t : time,
η : elevation of sea surface above mean sea level,
h : undisturbed water depth,
H : total water depth ($=h+\eta$)
A : horizontal eddy viscosity,
g : gravitational acceleration,
ω : angular velocity of the earth ($f=2\omega\sin\phi$),
R : radius of the earth,
P_a : sea surface pressure,
ρ : density of sea water,
$\tau\theta_s$, $\tau\phi_s$: θ and ϕ components of sea surface wind stresses,
$\tau\theta_B$, $\tau\phi_B$: θ and ϕ compoents of sea bottom stresses.

The bottom stresses are calculated as

$$\tau\theta_B = \frac{\rho k U (U^2+V^2)^{1/2}}{h+\eta},$$

$$\tau\phi_B = \frac{\rho k V (U^2+V^2)^{1/2}}{h+\eta} \qquad (6)$$

where k is the sea bottom frictional coefficient.

The sea surface stresses can be obtained as

$$\tau_s = \rho_a C_D W|W|, \qquad (7)$$

here, W is a wind velocity, ρ_a the air density(1.2 Kg m^{-3}), and C_D the wind drag coefficient ($=(0.8+0.065W)\times10^{-3}$, W in m/s; Wu, 1980, 1982).

B. The Model Area

The model area includes the entire coast of Korea: the Yellow Sea, the East China Sea, and a part of the East Sea (Fig. 1). This area covers 117° E.-134° E. in longitude and 24° 34′ N. – 43° 24′ N. in latitude. It consists of 66 by 83 grids. There are three segements of open boundary, north-eastern part of the East Sea, south-eastern part of the East China Sea, and southern part of the East China Sea. Most area of the model domain is a continental shelf. Relatively shallow depth exists near the south-eastern open boundary around the Ryukyu Islands.

C. Initial and Boundary Conditions

Initially the computation starts from a resting state, $\eta = U = V = 0$ at $t = 0$. It starts two days before the period of interest time.

The model is set for the disturbances which were developed in the model domain to propagate freely through open boundary by using the radiative boundary condition (Reid and Bodine, 1968; Flather and Davies, 1976).

$$Q_n = (gh)^{1/2}(\eta - \eta_m), \qquad (8)$$

where Q_n is the outward normal transport across the open boundary. Here it is assumed that internally generated disturbances can be represented as a progressive plane wave travelling at right angles to the open boundary. η_m represents the externally generated surge elevation entering the model area.

$$\eta_m = (P_n - P_a)/\rho g, \qquad (9)$$

here, P_n is the ambient mean sea surface pressure, 1010 mb for the summer typhoon seasons and 1025 mb for the winter storm season.

Along land boundaries, non-slip condition is

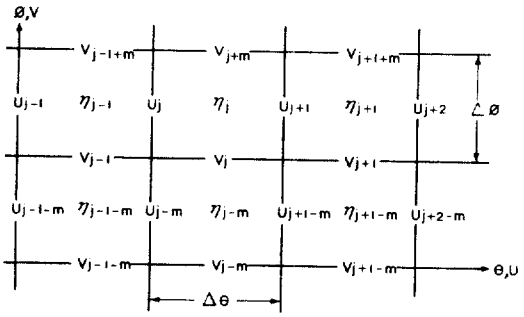

Fig. 2. Finite difference grid system ($\Delta\theta = 0.25°$ in longitude, $\Delta\phi = 0.2°$ in latitude, and m = number of grids in θ-direction).

applied, i.e., the velocities, u and v are assumed to be zero.

D. Finite Difference Equations

The finite difference scheme for the present study is sketched in Fig. 2. The equations(1)-(3) are read in difference form as follows,

$$\frac{\eta_{j,n+1}-\eta_{j,n}}{\Delta t}=\frac{-1}{R\cos\phi_j}\left\{\frac{\bar{H}^{\theta}_{j+1}U_{j+1}-\bar{H}^{\theta}_{j}U_j}{\Delta\theta}+\frac{\bar{H}^{\phi}_{j+m}V_{j+m}\cos\phi_{j+m}-\bar{H}^{\phi}_{j}V_j\cos\phi_j}{\Delta\phi}\right\} \quad (10)$$

$$\frac{U_{j,n+1}-U_{j,n}}{\Delta t}=2\omega\sin\phi_j\,\tilde{V}_j-\frac{g}{R\cos\phi_j}\frac{(\eta_{j,n+1}-\eta_{j-1,n+1})}{\Delta\theta}-\frac{kU_j(U_j^2+\tilde{V}_j^2)^{1/2}}{\bar{H}^{\theta}_{j}}+\frac{\bar{\tau}\theta_j}{\rho\bar{H}^{\phi}_{j}}-\frac{Pa_j-Pa_{j-1}}{\rho R\cos\phi_j\Delta\theta}-\frac{U_j(U_{j+1}-U_{j-1})}{2R\cos\phi_j\Delta\theta}-\frac{\tilde{V}_j(U_{j+m}\cos\phi_{j+m}-U_{j-m}\cos\phi_{j-m})}{2R\Delta\phi}+\frac{A}{R^2}\left\{\frac{(U_{j-1}+U_{j+1}-2U_j)}{(\cos\phi_j\Delta\theta)^2}-\frac{(U_{j+m}-U_{j-m})}{2\cot\phi_j\Delta\phi}+\frac{(U_{j-m}+U_{j+m}-2U_j)}{(\Delta\phi)^2}\right\}. \quad (11)$$

$$\frac{V_{j,n+1}-V_{j,n}}{\Delta t}=-2\omega\sin\phi_j\,\tilde{U}_j-\frac{g}{R}\frac{(\eta_{j,n+1}-\eta_{j-m,n+1})}{\Delta\phi}-\frac{kV_j(V_j^2+\tilde{U}_j^2)^{1/2}}{\bar{H}^{\phi}_{j}}+\frac{\bar{\tau}^{\phi}_{j}}{\rho\bar{H}^{\phi}_{j}}-\frac{Pa_j-Pa_{j-m}}{\rho R\Delta\phi}-\frac{\tilde{U}_j(V_{j+1}-V_{j-1})}{2R\cos\phi_j\Delta\theta}-\frac{V_j(V_{j+m}-V_{j-m})}{2R\Delta\phi}-\frac{\tilde{U}_j^2\tan\phi_j}{R}+\frac{A}{R^2}\left\{\frac{(V_{j-1}+V_{j+1}-2V_j)}{(\cos\phi_j\Delta\theta)^2}-\frac{(V_{j+m}-V_{j-m})}{2\cot\phi_j\Delta\phi}+\frac{(V_{j-m}+V_{j+m}-2V_j)}{(\Delta\phi)^2}\right\} \quad (12)$$

For the ϕ-directional momentum equation, the latitude ϕ_j is replaced by $\phi_j - \frac{1}{2}\Delta\phi$. The average operators are

$$\bar{H}^{\theta}_{j}=(H_j+H_{j-1})/2$$
$$\bar{H}^{\phi}_{j}=(H_j+H_{j-m})/2$$
$$\bar{\tau}^{\theta}_{j}=(\tau_j+\tau_{j-1})/2$$
$$\bar{\tau}^{\phi}_{j}=(\tau_j+\tau_{j-m})/2$$
$$\tilde{U}_j=(U_j+U_{j-m}+U_{j-m+1}+U_{j+1})/4$$
$$\tilde{V}_j=(V_j+V_{j+m}+V_{j+m-1}+V_{j-1})/4.$$

The governing equations were numerically integrated using a forward time scheme on a staggered spatial grid. Spatial grid intervals are 0.25° in east-west direction (= $\Delta\theta$), and 0.2° in north-south direction (= $\Delta\phi$), respectively. The CFL condition for computational stability requires that the time interval Δt is no greater than 90 seconds. The actual Δt used is 60 seconds, water density ρ, 1.0g/cm^3, gravitational acceleration g, 980 cm/sec^2, bottom frictional coefficient k, 0.0025 and horizontal eddy viscosity A, 10^6 cm^2/sec.

E. Meteorological Conditions

If one wants to simulate the actual situation of a storm surge field more accurately, the

carefully measured actual pressure and wind fields are essential. The real field data, however, are very difficult to obtain in severe situations like a storm. Even though we had some wind data which were obtained in these situations, they may not be dense enough to be used directly for the present model.

There are two indirect methods to obtain a wind field from air pressure data. The first method is to model the sea surface wind using several oceanic and meteorological parameters (Cardone, 1969; see Appendix). This method was used for winter storm in the present study. The second method is to get the sea surface wind from the sea surface pressure distribution under the assumption of geostrophic balance including a proper friction.

In a tropical cyclone structure the low-level (Ekman boundary layer) flow relative to the storm (the relative flow is obtained by subtracting the storm's velocity from the actual wind field) is approximately symmetric about the center of the storm, though in the upper layer (troposphere) the outflow is quite asymmetric (Anthes, 1982). This low-level symmetry is related to the strong circular isobaric field and the resulting symmetric pressure gradient force. Thus the surface pressure pattern of a typhoon shows close concentric circles. The associated wind fields are also closely related with these close pressure pattern. This symmetric field can be easily calculated by several parameters such as the air pressure of storm center and the radius of maximum wind.

There are several frequently used analytic models about air pressure distribution (Fujita, 1952; Myers, 1957; Holland, 1980). Holland (1980) reviewed these widely used analytic models including the two models above. His analytic model reads as,

$$P = P_c + (P_n - P_c)\ \exp(-A/r^B), \tag{13}$$

where P is the air pressure at a distance r from the storm center, P_c the pressure at the center, P_n the ambient pressure, and A,B are the parameters which determine the shape of the radial profiles of pressure and its gradient. From this pressure distribution, we can get the gradient wind as,

$$W = [AB(P_n - P_c)\exp(-A/r^B)/\rho_a r^B + r^2f^2/4]^{1/2} - rf/2, \tag{14}$$

using $dW/dr = 0$, we can find the radius of the maximum wind, R_o.

$$R_o = A^{1/B}. \tag{15}$$

According to Holland(1980), dimensionless parameter B is in the range of 1 – 2.5. For the present study, we choose 1. In this case R_o becomes A and this model becomes identical to the Myers'.

Since the air pressure of the typhoon center and the radius of the maximum wind vary with time, we supplied the locations and the air pressures of the typhoon center every 6 hours which were read from the weather charts of the area. From the center pressure and the surrounding pressure we obtained the radius of maximum wind. For actual calculations, the values are interpolated to make 30-minute interval data, considering the moving speed of the typhoons and the grid size of the present model. Table 1 shows the informations about the typhoons: Brenda, Vera and Thelma.

For actual computations, we considered the frictional effect of the sea surface in addition. Thirty percent reduced wind speeds and the corrected wind directions of 30° ingress angle to the typhoon center were used. In the Northern Hemisphere, the wind speeds of typhoon are stronger in the righthand side than in the lefthand side due to the translation of typhoon. In the present model we added the typhoon velocity to the calculated gradient wind speed.

Table 1. Location, center pressure (P_c) and radius of maximum wind (R_o) of the typhoons: Brenda (1985), Vera (1986) and Thelma (1987)

Data	Time [GMT]	Lat. °N	Long. °E	P_c [mb]	R_o [km]
3 OCT. 1985	00Z	19.7	125.3	965.	64.5
3	12Z	21.6	123.3	965.	58.6
4	00Z	24.5	122.8	955.	64.8
4	12Z	27.6	123.6	960.	54.2
5	00Z	32.2	126.2	965.	73.2
5	12Z	35.0	130.0	980.	66.2
6	00Z	38.0	132.0	992.	70.8
6	12Z	40.5	133.0	986.	100.6
6	00Z	42.0	136.0	988.	65.1
25 AUG. 1986	00Z	24.0	133.6	945.	105.7
25	12Z	25.2	130.6	945.	92.6
26	00Z	26.0	127.7	950.	116.1
26	12Z	27.4	125.3	950.	101.8
27	00Z	28.7	124.2	960.	107.6
27	12Z	30.9	124.1	960.	120.8
28	00Z	33.7	125.8	960.	140.0
28	12Z	37.5	127.7	980.	253.7
14 JUL. 1987	00Z	24.4	125.2	950.	56.1
14	12Z	27.1	125.1	950.	62.6
15	00Z	29.4	125.3	955.	65.2
15	12Z	33.9	127.2	965.	64.8
16	00Z	40.0	130.1	980.	146.3
16	12Z	43.0	132.0	988.	122.0

III. SIMULATION OF SURGES

1) Typhoon Periods

We simulated the storm surges generated in the periods of the three typhoons, Brenda (1985), Vera (1986) and Thelma (1987). Fig. 3 shows the tracks of the typhoons; after they passing the East China Sea, Brenda passed over the Korea Strait, Vera struck the south-western coast and Thelma approached the southern coast of Korea.

Using the sea level data obtained at tidal stations the surges (i.e., tide residuals) are calculated by eliminating the predicted tide which was composed of 64 tidal constituents. The tidal constituents are obtained by harmonic analysis using hourly sea level data of 355 days (See Oh, *et al.*, 1988).

A. Brenda

Brenda entered the model area at 00Z on October 4, 1985 and passed the study area from south-west to north-east direction. The model is set to run two days before the typhoon's entering the model area. At this initial stage the typhoon locates far out of the model area.

Fig. 4 shows the computed (dotted line) and the observed (solid line) surges during the Brenda period. The observed surges show about 1-day-peak instances, and several oscillations after the typhoon passage. The correlation coefficients between the observed and the computed surges are 0.49 (Daeheugsan), 0.87 (Cheju), 0.84 (Seogwipo), 0.54 (Yeosu), 0.68 (Keomundo), 0.41 (Chungmu), 0.37 (Pusan), 0.65 (Shimonoseki) and 0.46 (Nagasaki). Poor correlation coefficients seem to be due to mismatch in

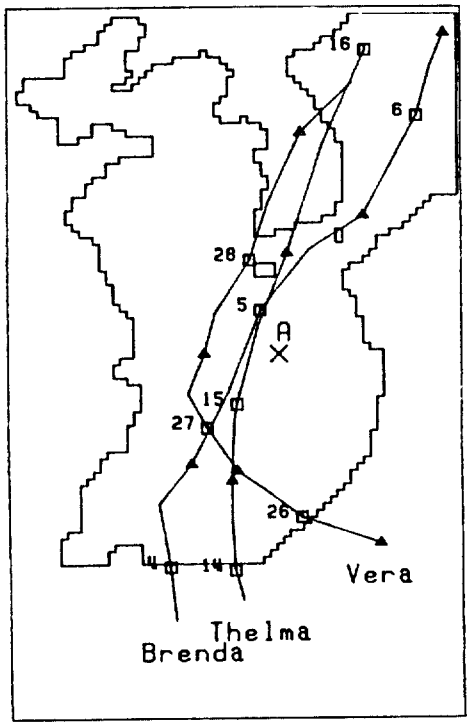

Fig. 3. Tracks of the typhoon Brenda (1985), Vera (1986) and Thelma (1987). The square is the position of the typhoon center at 00Z and the triangle at 12Z.

resurgence stage. Peak times of the surges match well in the western stations (Daeheugsan, Cheju and Seogwipo), but they tend to mismatch in the eastern stations such as Chungmu and Pusan. At Pusan the discrepancy is about 4 hours. There are two possible reasons for these. First, the position of the typhoon center is linearly interpolated from every 6-hour data in the model computation, thus the maximum discrepancy can be 6 hours. Second possible cause is the fact that the typhoon became a tropical depression during passage over the Korea Strait (from 12Z on October 5). During the process, the pressure and wind patterns are changed to the ones that could not match to our simple mathematical formula of pressure and wind fields.

B. Vera

Vera was a powerful typhoon. When she reached the Korean peninsular her center pressure was 960 mb, the maximum wind speed 70 m/s and the translation speed 10 km/h.

Fig. 5 shows the computed (dotted line) and observed (solid line) surges during the Vera period. Surges started increasing gradually from the time when the typhoon influenced the model area. Several high frequency oscillations which appeared in the recorded data are not simulated. At this moment, we do not know the reason, but we suppose that the tidal current may have done an important role. There are some experiments on the similar problem. According to Kim (1988), the interactions of surges and tides could generate such oscillations. Prandle and Wolf (1978) also reported that tidal frequences of M_2, M_4, M_6 etc. apprearing in surge profile were related to the residual component arising from modification of the tidal phase due to interaction with the surge. However, we need more data and experimental study to understand this problem.

The magnitudes and peak instances of the computed surges, however, agree well with those of the observed ones in this case. Correlation coefficients between the observed and the computed surges are 0.88 (Daeheugsan), 0.92 (Seogwipo), 0.71 (Cheju), 0.81 (Keomundo), 0.79 (Yeosu), 0.63 (Chungmu), 0.62 (Pusan), 0.73 (Shimonoseki), 0.76 (Fukue) and 0.75 (Nagasaki). The trends of the negative surge appeared at Daeheugsan and Seogwipo after their main peaks are simulated successfully. This negative surge seems to be related to the barotropic response of the ocean to a moving typhoon. This will be explained with the surge currents below.

The computed depth-mean currents and the computed sea level variations during the period of the typhoon Vera are shown in Fig 6a-f. The strong cyclonic wind during the typhoon period forces the sea water. Thus, the sea water moves in the same direction (Fig. 6a, c) and this cyclonic gyre induces negative sea level. As far as we know, there are no directly measured currents

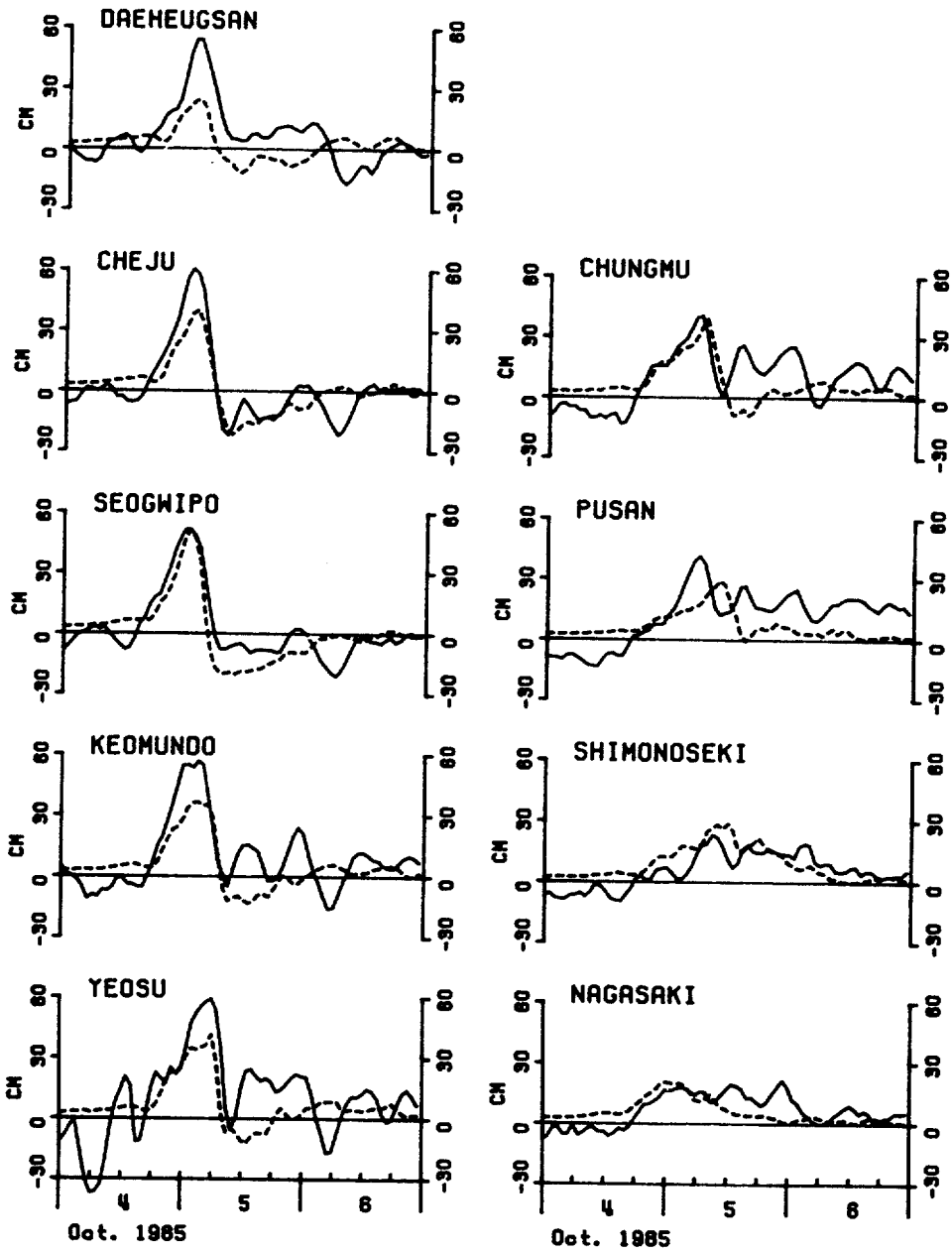

Fig. 4. Time series of the observed(solid line) and the computed (dotted line) surges during the typhoon Brenda. Time is the Greenwich means time.

and sea level data to compare with in this open sea area for the period.

We see that the center of the cyclonic gyre lies slightly behind the center of the typhoon (compare with the typhoon position in Fig. 3) and the center of the negative sea level also appears behind the center of the cyclonic gyre, while positive sea level appears at the center of the typhoon position due to the effect of the atmospheric pressure. At 00Z on August 28, the typhoon center locates at the northwest of the Cheju island, but the center of the cyclonic gyre

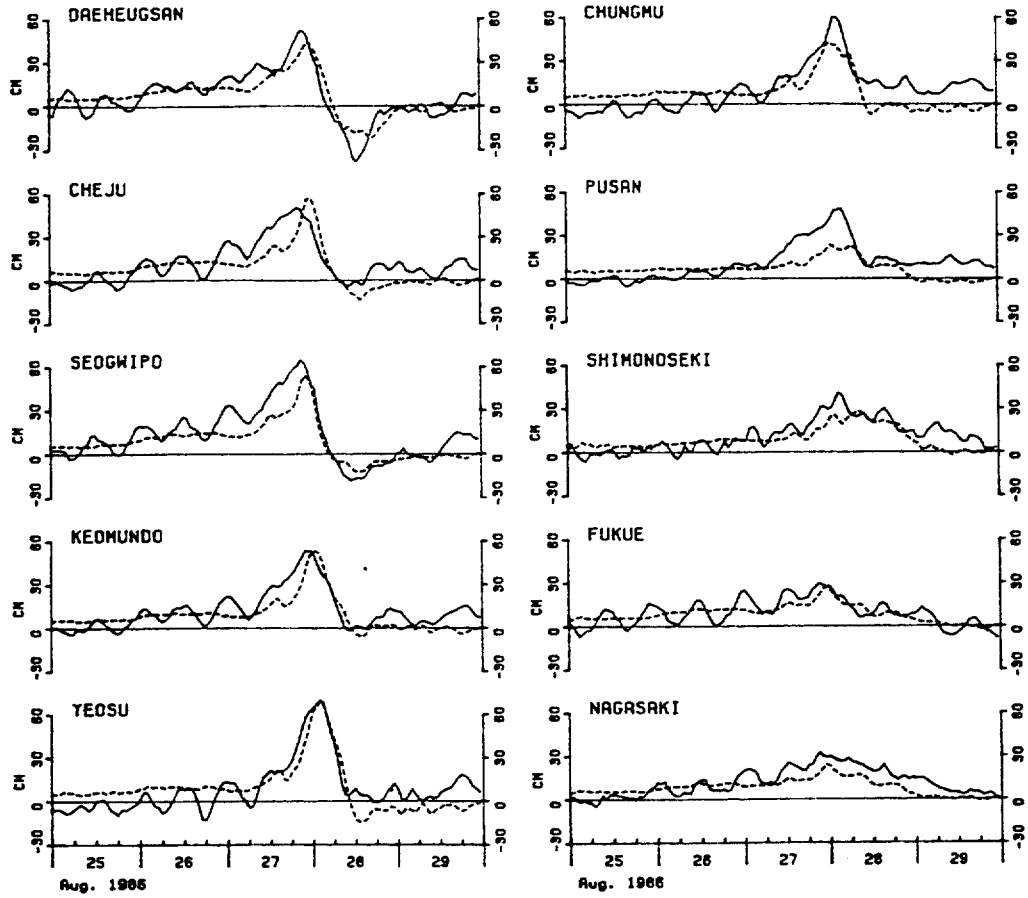

Fig. 5. Time series of the observed (solid line) and the computed (dotted line) surges during the typhoon Vera. Time is the Greenwich mean time.

is at the southwest of the island (Fig. 6 c). Negative sea level and cyclonic gyre are elongated following the typhoon. After 12 hours (12Z on August 28) the typhoon locates on the Korean peninsula, and the current strengths are weakened. The cyclonic gyre lasts quite a long time after the typhoon passes the area. The shape of the elongated gyre matches the contour of the sea level. It seems that the surge currents flow along the contour lines at this time. This means that the cyclonic gyre of the sea water due to the wind forcing is balanced by pressure gradient forces and Coriolis forces in a quasi-geostrophic sense when meteorological forcing abates.

Similar phenomena are observed in open sea (O'Brien and Reid, 1967; Leipper, 1967; Geisler, 1970; Suginohara, 1973; Chang and Anthes, 1978; Greatbatch, 1984; Cooper and Thompson, 1989). It is known that the baroclinic and barotropic modes are induced when a typhoon passes over an ocean (See Anthes, 1982). The trough of the surface height (negative sea level in the elongated gyre area in this study) generated by the wind stress curl is a barotropic mode (Geisler, 1970). Similar results are also found in the barotropic mode of Kuo and Ichiye (1977). Cooper and Thompson (1989), however, argued that the deep water response can be characterized as baroclinic in the sense that the response is dominated by effect of stratification and is largely independent of external presssure gradients, while the shallow water response can be charac-

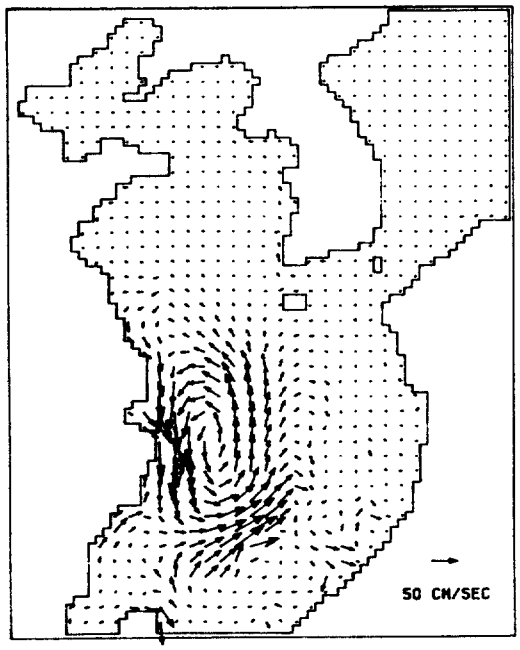

Fig. 6a. Computed depth-mean current field at 12Z August 27, 1986, during the typhoon Vera.

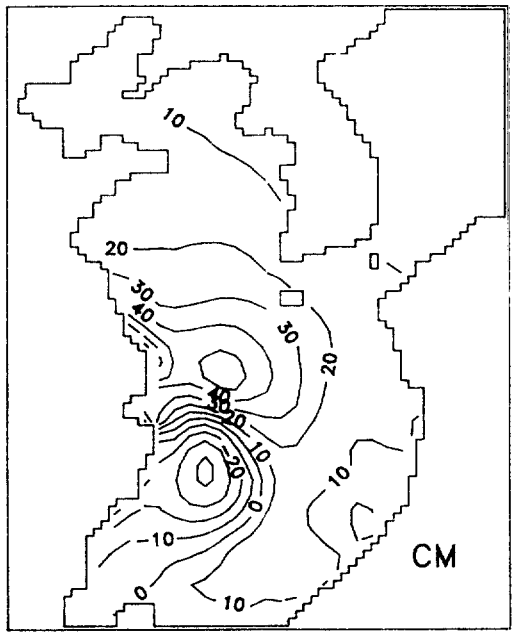

Fig. 6b. Computed sea level at 12Z August 27, 1986, during the typhoon Vera.

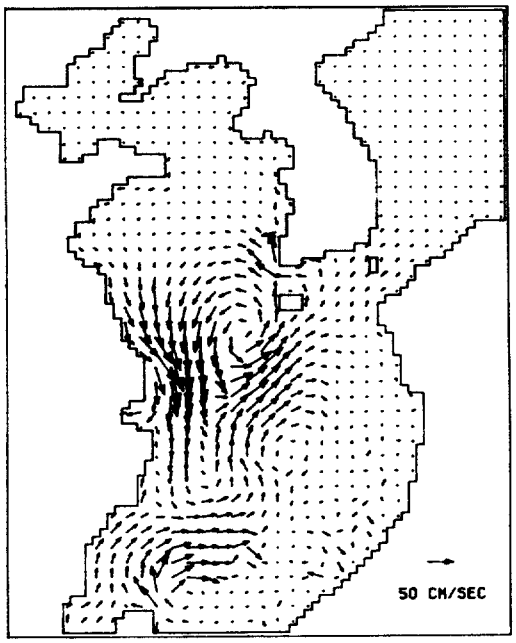

Fig. 6c. Computed depth-mean current field at 00Z August 28, 1986, during the typhoon Vera.

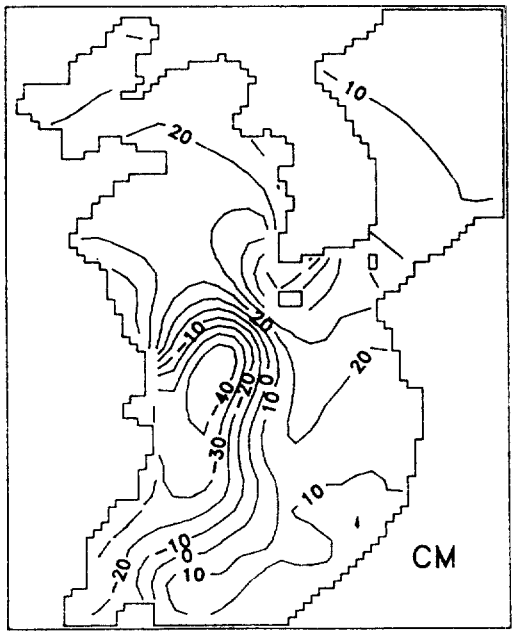

Fig. 6d. Computed sea level at 00Z August 28, 1986, during the typhoon Vera.

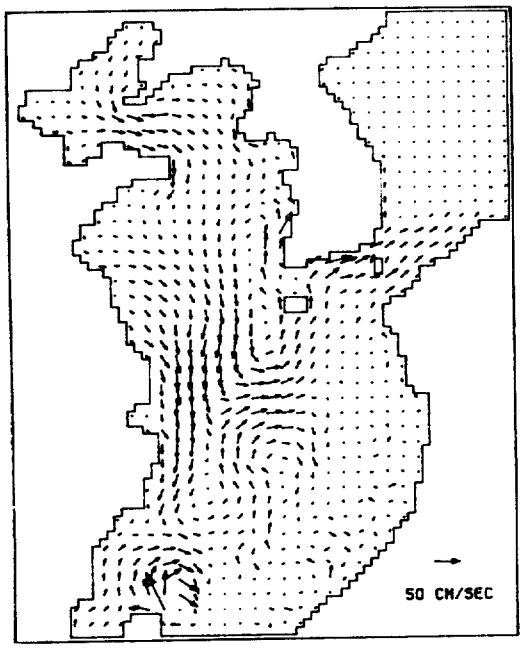

Fig. 6e. Computed depth-mean current field at 12Z August 28, 1986, during the typhoon Vera.

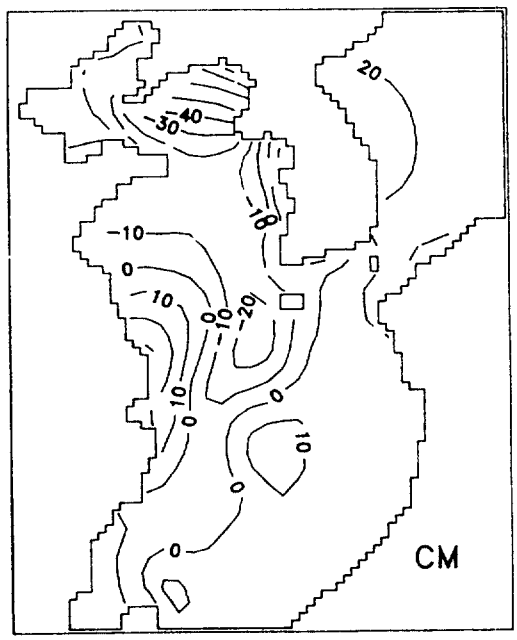

Fig. 6f. Computed sea level at 12Z August 28, 1986, during the typhoon Vera.

terized as barotropic, in the sense that the flow is slablike and internal pressure gradients are unimportant.

At this moment we don't know which process is more dominant than the other in our study area, continental shelf, because the present model has only one layer. But, it is certain that the negative surge appeared in coastal area after typhoon passing is closely related to the negative sea level induced by wind stress curl in open sea. This negative sea level area of open sea exists behind the typhoon because in the area, the influence of the wind-induced water circulation on sea level variation is stronger than that of sea surface air pressure. As the typhoon moves close to land and crosses the southern coast of Korea, the contoured shape of the negative sea level is more elongated, and the cyclonic water motion of the elongated gyre is hindered by land masses (the Korean Peninsular and Japan Islands). The sea water of the lefthand side of the gyre is drawn offshore, while the water of the right-hand side of the gyre piles up. Thus, the western staions, such as Daeheugsan, Seogwipo, show negative surges after the typhoon passing, but the eastern stations do not. We believe that this is not the only reason why the western stations have negative surges but, this explains, at least, why negative surges are relatively clear in the western stations while not in the eastern stations.

C. Thelma

Thelma was a fast moving typhoon with a translation speed 30 km/h, a wind speed of 35 m/s and a center pressure of 965 mb when the typhoon reached the southern coast of Korea. Unfortunately, no dependable data were collected for about two days due to the malfunctioning of the tide gauges. Thus, Fig. 7 shows only the computed surges during the Thelma period. Sharp peak instances shown in this figure are due to the typhoon's fast translation.

The computed depth-mean currents and the contours of the computed sea level during the

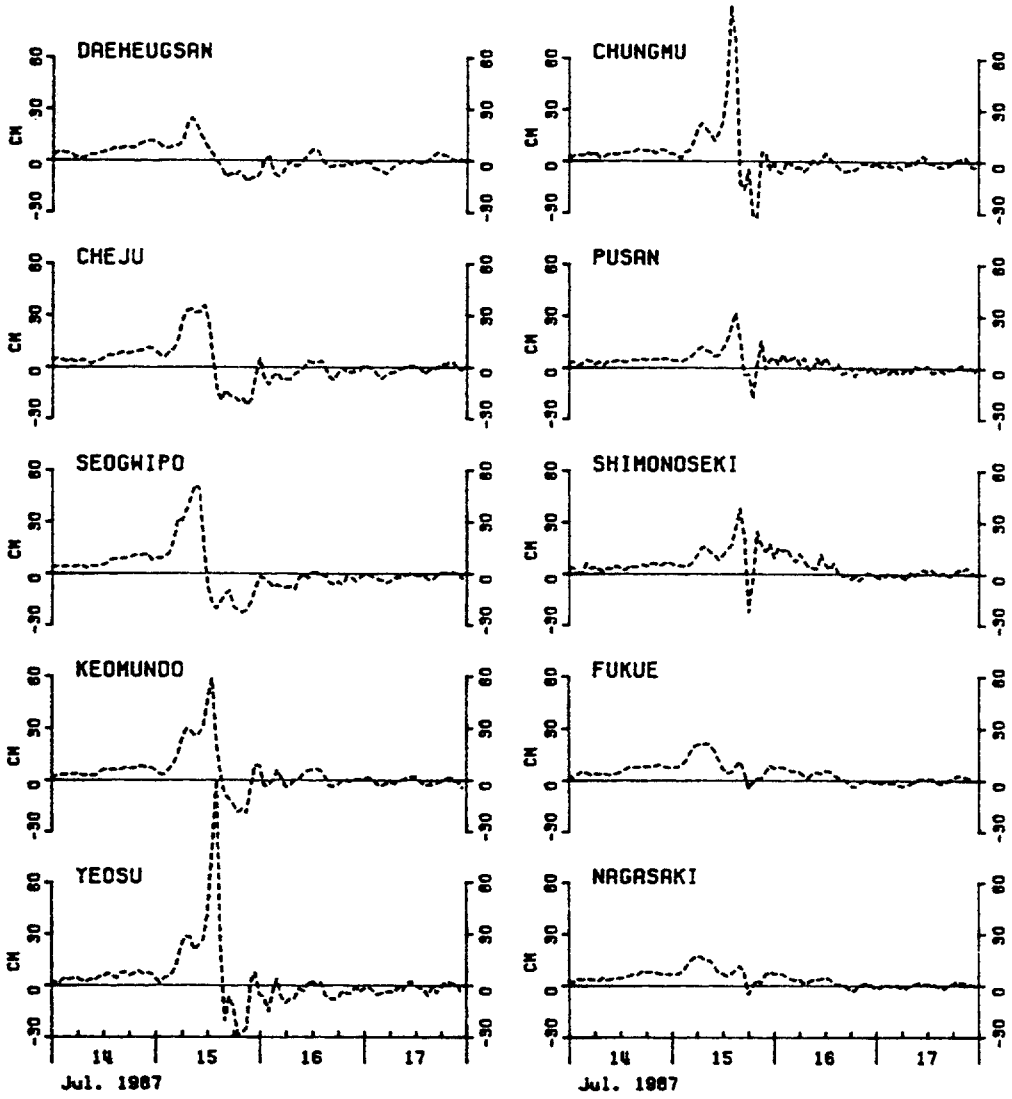

Fig. 7. Time series of the computed surges during the typhoon Thelma. Time is the Greenwich mean time.

period of Thelma are shown in Fig. 8. The cyclonic wind forcing piles up the sea water along the southern coast of Korea at 12Z on July 15, 1987. This causes the large computed surge at Yeosu and Chungmu (Fig. 7). The elongated gyre also appears in this event but the gyre is separated into two at 12Z on July 15. The stronger gyre locates at the position where the typhoon center is at 00Z on July 15 and lasts all through the computations. The center of the negative sea level is located at the same place until it disappears.

Fig. 9 shows the time series of force balance in ϕ-directional momentum equation in readjusting process after typhoon passing. The series are taken from a point, A, located at the righthand side of the typhoon track during ten days run (see Fig. 3 for the location of the point A). Four terms are dominant: Coriolis force (CF), pressure gradient force(PG), wind stress(WS) and sea surface air pressure gradient force (SAP). The other terms of the equation

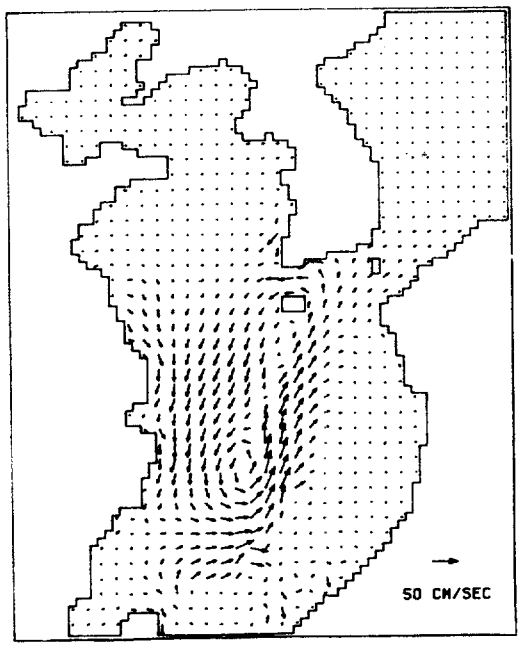

Fig. 8a. Computed depth-mean current field at 12Z July 15, 1987, during the typhoon Thelma.

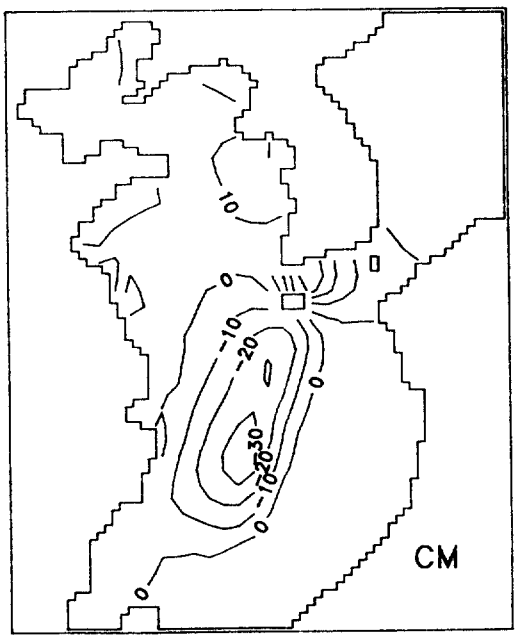

Fig. 8b. Computed sea level at 12Z July 15, 1987, during the typhoon Thelma.

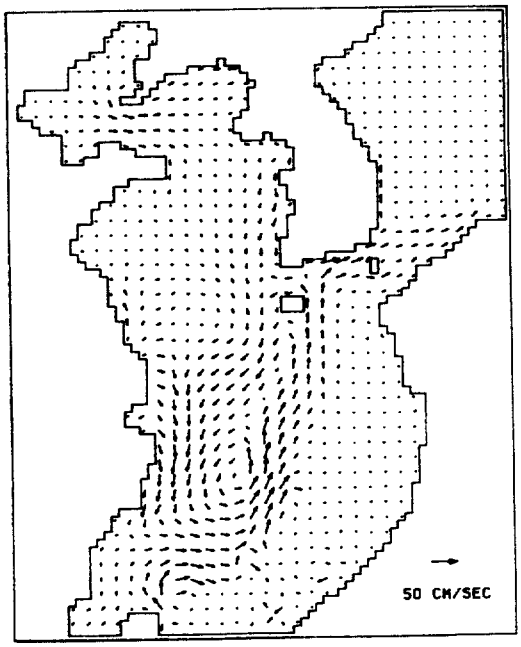

Fig. 8c. Computed depth-mean current fieldat 00Z July 16, 1987, during the typhoon Thelma.

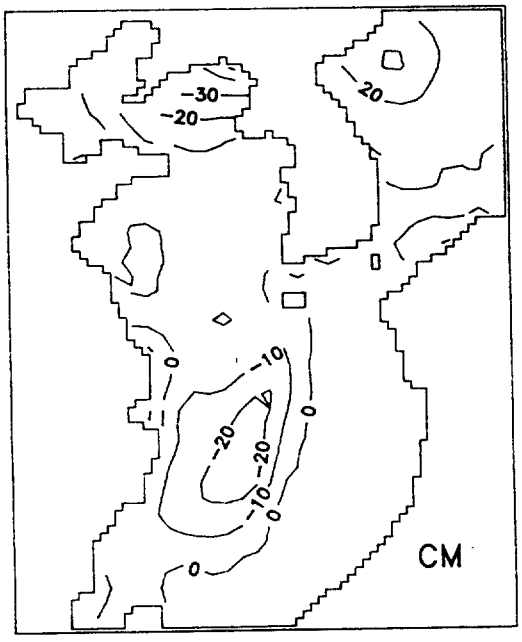

Fig. 8d. Computed sea level at 00Z July 16, 1987, during the typhoon Thelma.

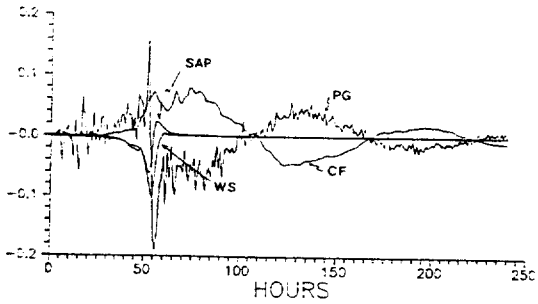

Fig. 9. Relative magnitudes of the dominant terms (CF: Coriolis force; PG: pressure gradient force; SAP: sea surface air pressure gradient; WS: wind stress) in ϕ-directional momemtum equation at a point (A) in the righthand side of a typhoon track (See Fig. 3 for the location).

are negligibly small (1 or 2 orders of magnitude less). The time variational term can be large when the four dominant terms are not balancing for the first 60 hours. Notable figure is the force balancing between CF and PG when SAP and WS are drastically reduced. It is interesting that the force balance between CF and PG is achieved whether the Coriolis force is negative or not. This fact supports that the force balance in readjusting stage becomes quasi-geostrophic.

2) Winter Storm

The storm surges generated during an extra-tropical cyclone passage in winter (Junuary 1-6, 1986) are simulated. The synoptic air pressure distribution for the area is as follows.

A low pressure with a center pressure 1018 mb is developed in the northwest of the Korean Peninsula near the Pohai Sea at 12Z on January 2 (see Fig. 10). This low pressure moved eastward by crossing the northern part of the Peninsula, and strengthened its influence with a center pressure 1008 mb at 00Z on January 3. At 00Z of the next day, this low pressure center located in the middle of the East Sea. Meanwhile, a high pressure which was near the Pohai Sea moved closer to the Peninsula with a center pressure 1032 mb. Due to this pressure pattern, close isobars were shown in the north-south direction, and the associated strong winds (about 10-18 m/sec) were recorded in the Yellow Sea on January 4 and 5.

In order to compute the sea level variations under this meteorological condition by the present model, it is necessary to input sea surface winds. We obtained the sea surface wind distributions from a numerical model established by Bong, *et al.* (1988, 1989). This sea surface wind model generally follows the logic of Cardone(1969). A brief description of the model is in the Appendix of the present paper.

Fig. 11 shows the computed (dotted line), the observed (solid) and the moving averaged observed (dashed) surges. After positive surges on January 2 and 3, negative surges were recorded. Surges get smaller from Inchon to Daeheugsan, especially the negative surges. The negative surge is coincident to the close isobars which appeared in the Yellow Sea (see Fig. 10). By the model test, we found that the magnitudes of negative surge are proportional to the southward wind strength. Model result shows a similar pattern to the 13-hour moving averaged observed data rater than to the observed data themselves. The high frequency oscillations (about 12 hours) seen in the observed data are not simulated properly. However, the correlation coefficients between the moving averaged and the computed surges shows fair agreements, i.e., 0.82, 0.66, 0.68 and 0.64 for Inchon, Kunsan, Mokpo and Daeheugsan, respectively.

There are two possible reasons on this considerable discrepancies between the observed and the computed surges. The first one is due to the insufficiency in sea surface wind. The temporal and space resolution of the wind data is not dense enough. The time resolution of the wind data is 12 hours, while the time step of the present model is 60 seconds. The space resolution of the wind data may also cause some errors. The resolution of the wind data is about 200 km, while the grid size of the present surge model is about 22 km. The other reason can be the tidal effects. The presence of tides could

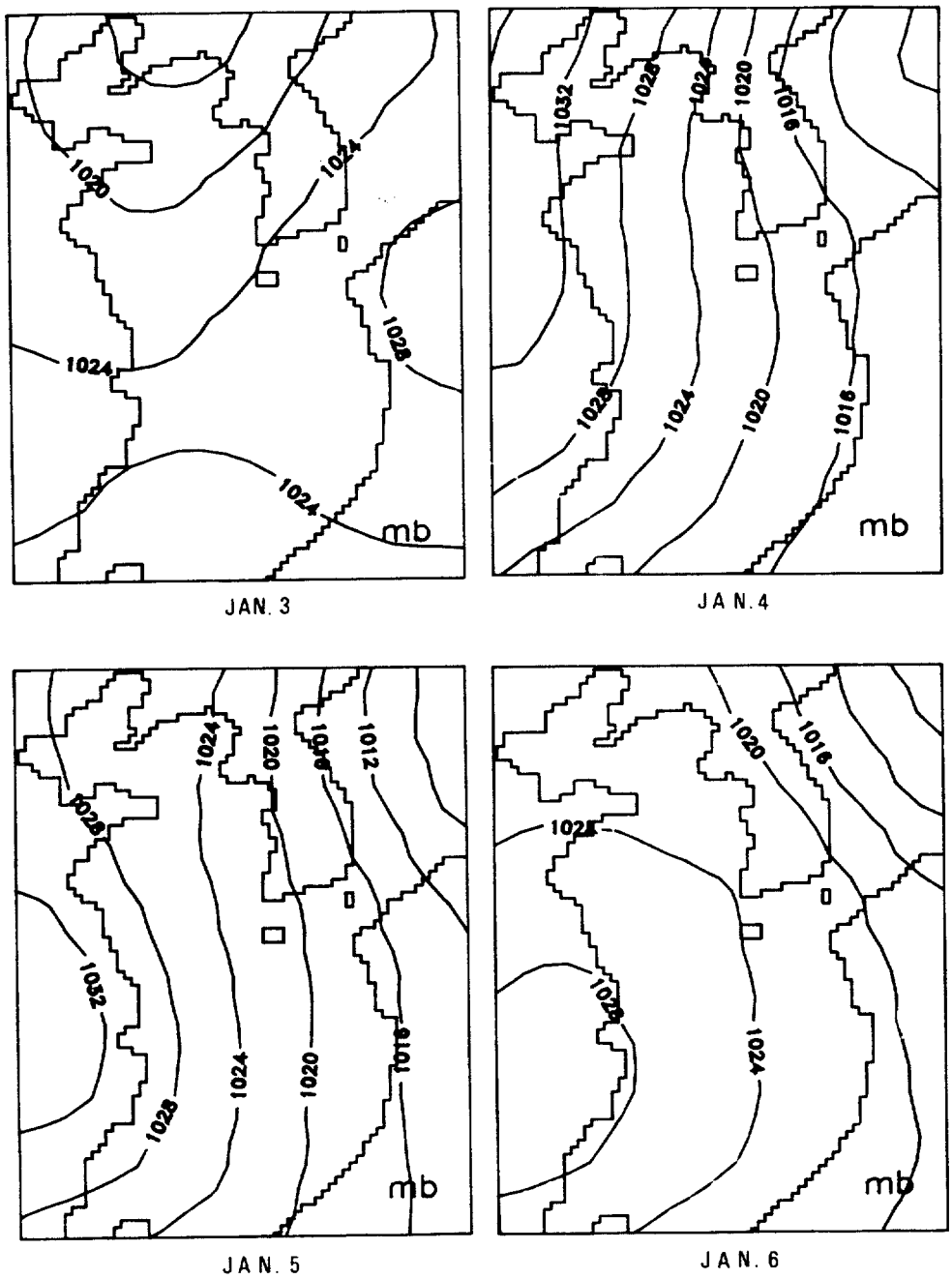

Fig. 10. Sea surface pressure distributions at 00Z, January 3-6, 1986.

make a considerable difference in the surge profile as mentioned in the previous section(Choi, 1986; Kim, 1988), but we did not consider the tidal effects in this study. We reserve this problem for the next target.

The depth-mean current fields and sea level variations at every 12-hour interval are shown in Fig. 12. The northerly wind generates southward flows in most parts of the Yellow Sea (Fig. 12 a,c). The outward flow from the Yellow sea

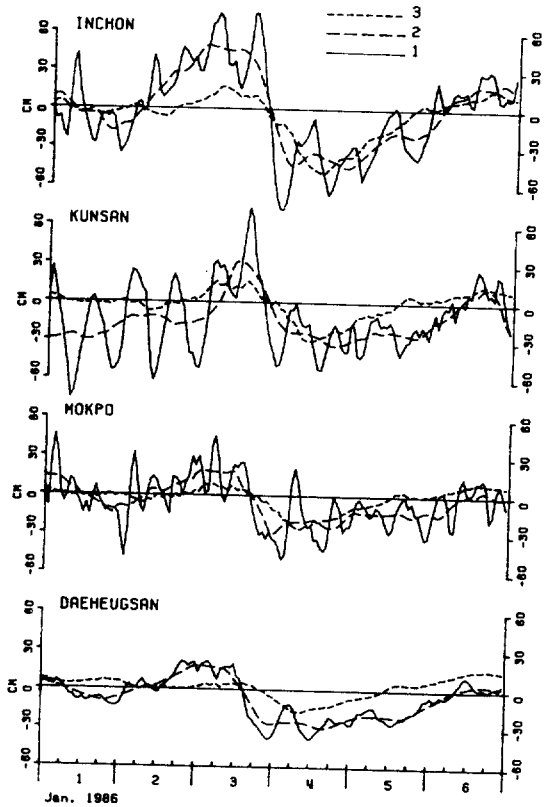

Fig. 11. Time series of the observed (1), the 13-hour averaged (2) and the computed (3) surges during the typhoon Thelma. Time is the Greenwich mean time.

causes the sea level drop in the northern reach (Fig. 12 b,d). The southward wind forcing becomes stronger from south (East China Sea) to north (Yellow Sea) after the low pressure passage. Consequently a sea level setup is made from the Yellow Sea to the East China Sea. Similar setup along the west coast of Korea is repoted by Hsueh, *et al.* (1986). According to them, the presence of sea level setup along the west coast of Korea is a consequence of the presence, at the end of the peninsula, of relatively deep offshore water that was less responsive to wind forcing than the shallow shelf water.

The negative surge and the increase in its magnitude from south to north along the west coast of Korea (see Fig. 11) can be attributed to

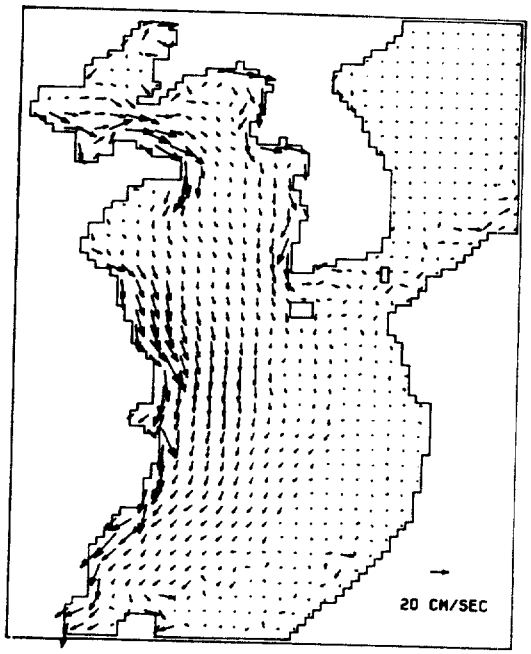

Fig. 12a. Computed depth-mean current field at 00Z January 4, 1986, during winter storm.

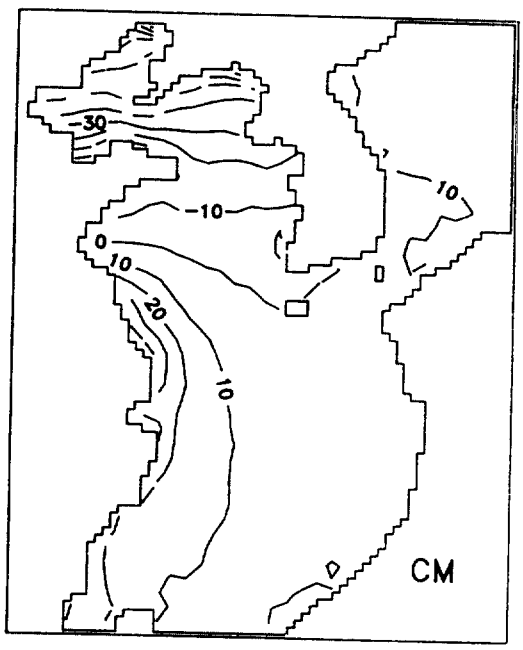

Fig. 12b. Computed sea level at 00Z January 4, 1986, during winter storm.

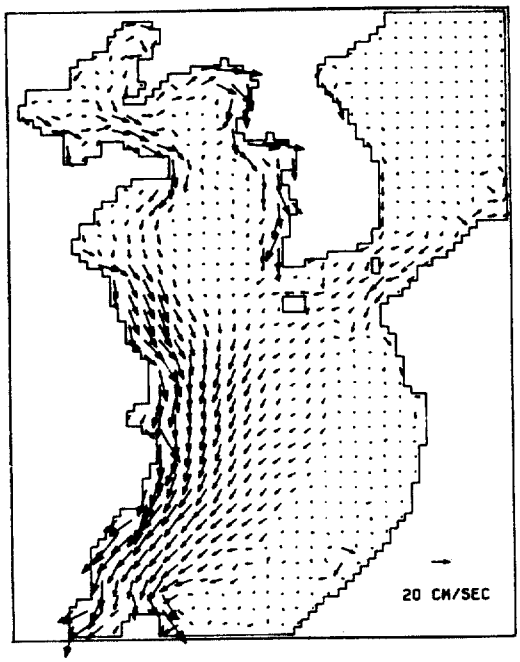

Fig. 12c. Computed depth-mean current field at 12Z January 4, 1986, during winter storm.

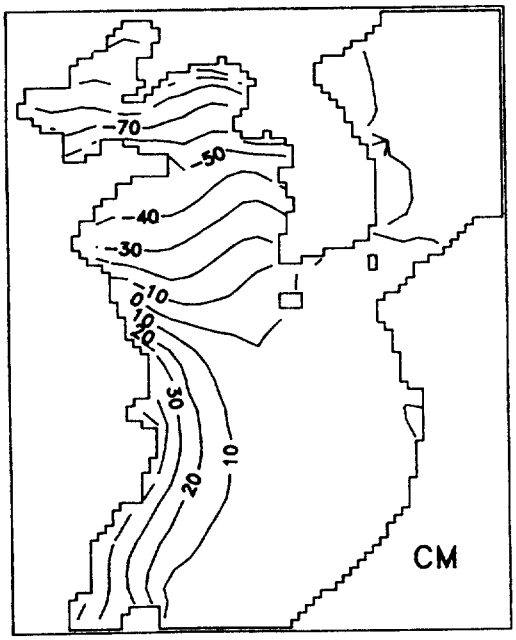

Fig. 12d. Computed sea level at 12Z January 4, 1986, during winter storm.

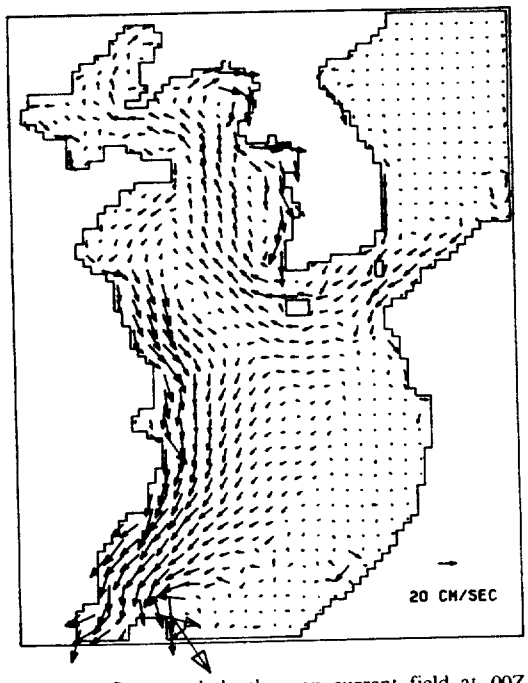

Fig. 12e. Computed depth-mean current field at 00Z January 5, 1986, during winter storm.

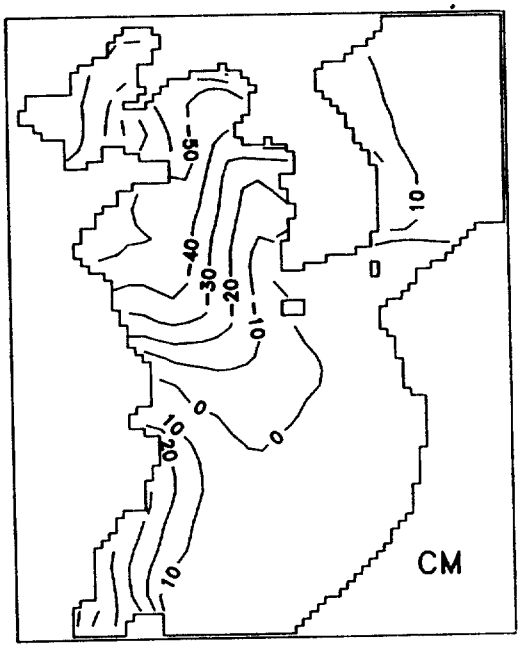

Fig. 12f. Computed sea level at 00Z January 5, 1986, during winter storm.

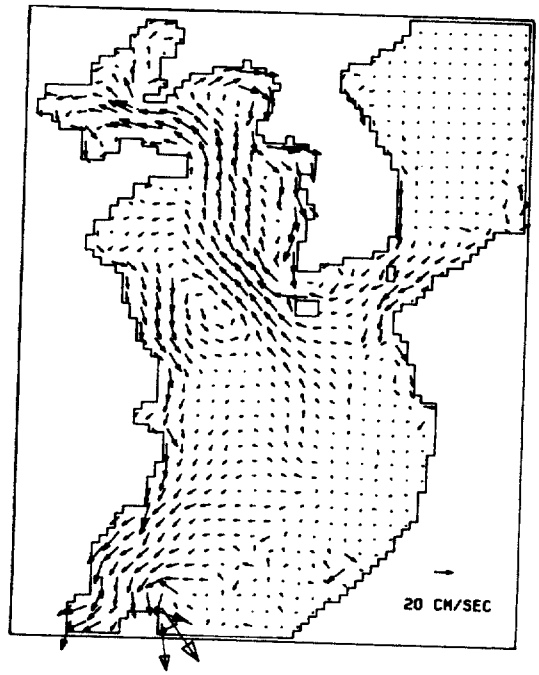

Fig. 12g. Computed depth-mean current field at 12Z January 5, 1986, during winter storm.

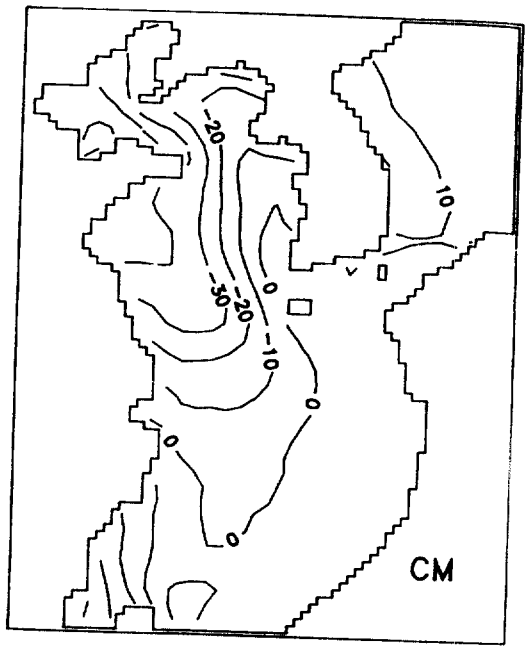

Fig. 12h. Computed sea level at 12Z January 5, 1986, during winter storm.

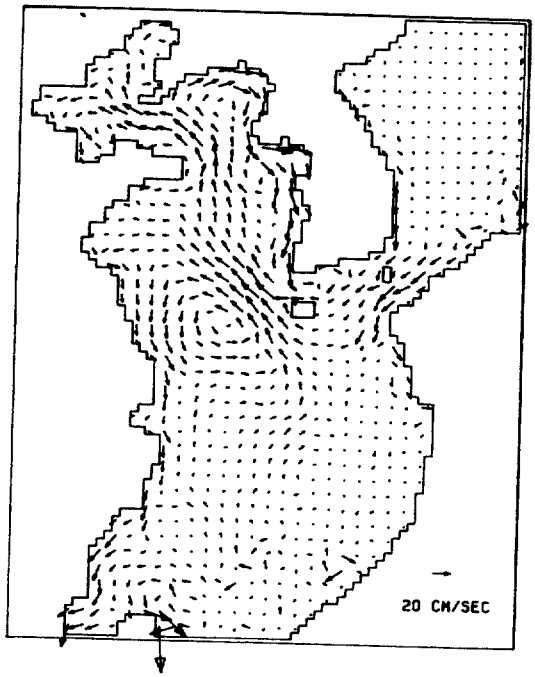

Fig. 12i. Computed depth-mean current field at 00Z January 6, 1986, during winter storm.

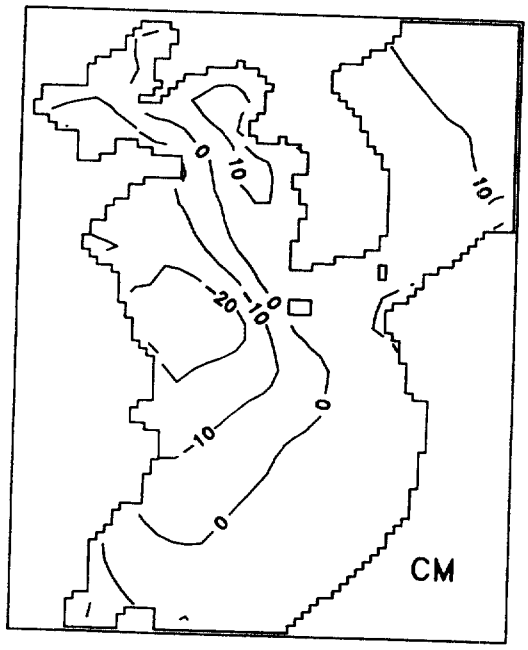

Fig. 12j. Computed sea level at 00Z January 6, 1986, during winter storm.

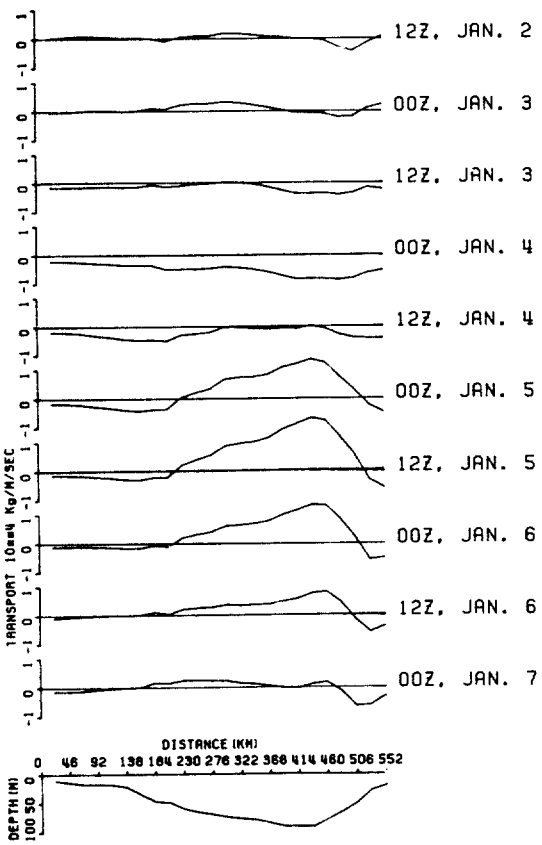

Fig. 13. Computed north-southward transport (positive northward) through the east-west line connecting the southmost point of the Korean Peninsular with China during winter storm.

this sea level setup to south. When the northerly wind abates, northward (upwind) flow begins to appear in more deep part of the Yellow Sea, yet southward flow continues in more shallow parts of the sea (Fig. 12. e,g,i). Due to the northward flow, the sea level begins to ascend first in the eastern part of the Yellow Sea (Fig. 12. f,h,j). North-southward transport through the east-west line connecting the southmost point of the Korean Peninsula with China shows in/outward flow pattern druing the process (Fig. 13). Southward flow exists throughtout the entire section. The maximum transport is formed in the trough of the Yellow Sea. Northward flow appeares in a great magnitude at the trough of the Yellow Sea from January 5, while southward flow continuously apprears in the adjacent areas of China and Korea, i.e., in the relatively shallow water. At January 7, a considerable southward flow is appeared along the Korean coast. It makes the net transport of the whole cross section vanish. From this analysis, we found that in/outward flows mainly exist in the trough of the Yellow Sea, while some waters in shallower area flow in opposite direction.

IV. CONCLUDING REMARKS

We simulated the storm surges which were occurred in the seas around Korea. The generated storm surges are in two categories: one is a surge due to a typhoon in summer and the other is due to an extratropical cyclone in winter.

The surge simulations for typhoon seasons show good agreements with the observed ones. However, the simulations of the winter seasons' show considerable discrepancies.

From the surge simulations, we found some interesting features in our shallow study area. A negative sea level is clearly shown behind the positive sea level which are directly underneath the typhoon center. As the typhoon move closer to a land boundary, the negative sea level are hindered to 'follow' the storm because the surges are strongly related to the sea water movement. Considering the typhoon direction crossing the southern coast of Korea from the south, we can understand why the western stations usually have clear negative surges while the eastern stations do not.

The shape of this negative sea level becomes elongated as time goes by. The balance of forces which control the seawater motion in open sea is maintained by Coriolis force and pressure gradient force. This balance of forces could be quite different in a shallow area and in a coastal region. Bottom and lateral friction term will be more important.

There could be many problems in surge simulation, especially for winter season cyclones. Among them, a very important and inevitable

problem is due to an insufficient accuracy in sea surface wind.

The magnitude and peak time of a calculated surge are strongly dependent on the center pressure and the track of the storm considered. Therefore, an exact prediction of a storm surge needs correct informations of the strom.

This model does not include any surge-tide and surge-wave interactions. We, however, believe that tidal current would play an important role in generating the high frequency oscillations of surge which were appeared in the recored surge, and the tide itself be modified somewhat. We have already made a good progress on this proglem and will conduct more experiments on it.

ACKNOWLEDGEMENTS

The authors appreciate the careful reading and comments of Prof. S.R. Lee on the earlier draft of this paper. The authors would also like to thank the researchers of the Hydrographic Office, Ministry of Trasnsportation for providing the valuable sea level data. This work was supported in part by the Ministry of Education through the Basic Science Research Program, 1988-1989 and by the Ministry of Science and Technology through the Meteorological Research Institute, 1987-1989.

APPENDIX
SEA SURFACE WIND MODEL

Cardone(1969) separated the atmospheric boundary into surface and Ekman layers. He assumed that at the upper limit of the Ekman layer the wind velocity becomes the geostrophic wind i.e., $V = V_g$, and in surface layer the wind velocity has a logarithmic profile and it vanishes at the sea surface(Fig. A1).

The variables are

W : wind velocity in Ekman layer, and $W_h = W(z=h)$

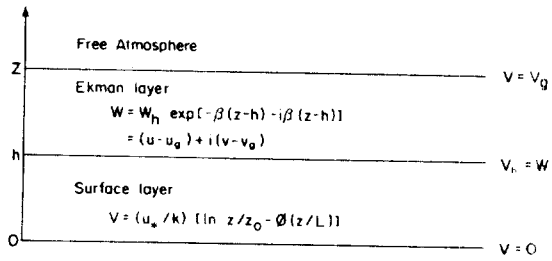

Fig. A1. Seperation of atmospheric boundary layer.

V : wind velocity in surface layer, and $V_h = V(z=h)$,

u_g, v_g: Eastern and Northern components of geostrophic wind V_g in free atmosphere, respectively,

u_* : frictional wind velocity,

k : von Karman constant ($=0.4$),

z_o : sea surface rougness,

ϕ : function concerning the vertical stability of atmosphere which is a function of Monin-Obukhov stability length, L,

β : $\sqrt{f/2\nu}$, where ν is eddy diffusion coefficient, and

h : height of surface layer.

The wind velocity in Ekman layer is obtained from the momentum equation as follows,

$$f\bar{k} \times \bar{V} = -\frac{1}{\rho}\nabla P + \frac{1}{\rho}\frac{\partial \tau}{\partial z},$$

where $\bar{V}$, P, ρ, f and τ are wind velocity, air pressure, air density, Coriolis parameter and wind stress, respectively.

The surface layer height is determined from $h = B_o V_g / f$, here B_o is a constant coefficient of 3×10^{-4}. The distributions of sea surface and air temperatures are used for the calculation of L (Kim, 1989).

Bong, *et al.* (1988, 1989) made a numerical model for the calculation of sea surface wind using the model above. For the present study, we used the sea surface wind model.

REFERENCES

Anthes, R.A., 1982. Tropical cyclones, their evolution,

structure and effects, American Meteorological Society, Meteorological Monographs 19(41), 208 pp.

Bong, J.H., J.B. Choi, I.S. Oh, I.S. Kang, Y.H. Yoon, S.I. Kim, T.R. Kim, K.M. Kim, J.k. Park, and H.J. Chung, 1988. The study of meteorological characteristics and marine forcasting over the seas around Korea (II). Meteorological Research Institute, Korea Central Meteorological Service. Report, 323 pp.

Bong, J.H., J.B. Choi, I.S. Oh, I.S. Kang, Y.H. Yoon, S.I. Kim, T.R. Kim, K.M. Kim, M.K. Kim, and H.J. Chung, 1989. The study of meteorological characteristics and marine forecasting over the seas around Korea (III). Meteorological Research Institute, Korea Central Meteorological Service. Report, 355 pp.

Cardone, V.J., 1969. Specifiation of the wind distribution in the marine boundary layer for wave forecasting, New York Univ. School for Engineering and Science. Rep. TR-1, 181 pp.

Chang, S.W., and R.A. Anthes, 1978. Numerical simulations of the ocean's nonlinear, baroclinic response to translating hurricanes, *J. Phys. Oceanogr.*, **15**: 1847-1858.

Choi, B.H., 1986. Surge hindcast in the East China Sea, *Prog. Oceanogr.*, **17**: 177-192.

Chu, G.S., 1987. On the storm surges and tsunami occurred in the coast of Korea, Hydrographic Office, Republic of Korea, 153 pp.

Cooper, C. and J.D. Thompson, 1989. Hurricane-generated currents on the outer continental shelf, 1. Model formulation and verification. *J. Geophys. Res.*, **94**(C9): 12513-12539.

Flather, R.A. and A.M. Davies, 1976. Note on a preliminary scheme for storm surge prediction using numerical models. *Q.J.R. Meteorol. Soc.*, **102**(431): 123-132.

Fujita, T., 1952. Pressure distribution in typhoon, *Geophys. Magazine*, 23.

Geisler, J.E., 1970. Linear theory of the response of a two-layer ocean to a moving hurricane, *Geophys. Fluid Dyn.* **1**: 249-272.

Greatbatch, R.J., 1984. On the response of the ocean to a moving storm: parameters and scales, *J. Phys. Oceanogr.*, **14**: 59-77.

Holland, G.J., 1980. An analytic model of the wind and pressure profiles in hurricanes. *Mon. Wea. Rev.*, **108**: 1212-1218.

Hsueh, Y., R.D. Romea and P.W. deWitt, 1986. Wintertime winds and coastal sea-level fluctuations in the Northeast China Sea. Part II : Numerical Model. *J. Phys. Oceanogr.*, **16**: 241-261.

Hwang, J.P., 1971. On the variation of sea level due to meteorological disturbances of the coast of Korea. 1. Storm surges caused by typhoon Billie, 1970, on the west and south coasts of Korea, *J. Oceanol. Soc. Korea*, **6**: 92-98.

Kim, S.I., 1988. A study on the sea level variations caused by the typhoon passing thrgough the South Sea of Korea, MS Thesis, Departemnt of Oceanography, Seoul National University. 70 pp.

Kim, K.M., 1989. Sea surface wind model around the Korean Peninsular, MS thesis, Department of Atmospheric Sciences, Seoul National University. 76 pp.

Korean Central Meteorological Service, 1984. Typhoon report of Korea 1904-1984. 364 pp.

Korea Ocean Research and Development Institute, 1985. A study on marine forecasting system for disaster prevention in Korea (I), BSPE 56-87-1.

Korea Ocean Research and Development Institute, 1986. A study on marine forecasting system for disaster prevention in Korea (II), BSPG 33-121-1.

Kuo, H.L., and T. Ichiye, 1977. A numerical study of the response of a barotropic ocean to a moving hurricane, *Tellus*, **29**, 561-571.

Leipper, D.F., 1967. Observed ocean conditions and Hurricane Hilda, 1964, *J. Atmos. Sci.*, **24**: 182-196.

Myers, V.A., 1957. Maximum hurricane winds, *Bull. Amer. Meteor. Soc.*, **38**: 227-228.

O'Brien, J.J., and R.O. Reid, 1967. The non-linear response of a two-layer, baroclinic ocean to a stationary, axially-symmetric Hurricane: Part 1. Upwelling induced by momentum transfer, *J. Atmos. Sci.*, **24**: 197-207.

Oh, I.S., S.I. Kim, and J.H. Bong, 1988. Storm surges by the typhoons passing through the South Sea of Korea. *J. of Korea Met. Soc.*, **24**(3): 72-84.

Prandle, D. and J. Wolf, 1978. The interaction of surge and tide in the North Sea and River Thames. *Geophys. J.R. astr. Soc.* **55**: 203-216.

Reid, R.O., and B.R. Bodine., 1968. Numerical model for storm surges in Galveston Bay. *Proc. Amer. Soc. Civ. Eng. J. Waterways Harbors Div.*, **94**(WW1): 33-57.

Suginohara, N., 1973. Response of a two-layer ocean to typhoon passage in the western boundary region, *J. Oceanogr. Soc. Japan*, **29**: 10-23.

Wu, J., 1980. Wind-stress coefficients over sea surface in neutral condition - a revisit. *J. Phys. Oceanogr.* **10**: 727-740.

Wu, J., 1982. Wind-stress coefficients over sea surface from breeze to hurricane. *J. Geophys. Res.* **87**: 9704-9706.

Received December 4, 1989
Accepted November 14, 1990